Three-Dimensional Combustor Performance Validation with High-Density Fuels

N. K. Rizk* and H. C. Mongia†
General Motors Corporation, Indianapolis, Indiana

A combustor performance model that utilizes the detailed representation of the flowfield made available through analytical three-dimensional codes and the predictive tool of the empirical correlations is validated with high-density fuels data. These data were obtained by burning four different fuel types that varied over a wide range of physical and chemical properties in addition to a baseline JP-4 fuel, in a single-can combustor rig. The predictions of the combustor model agree fairly well with the experimental data. Wall temperature predictions were made through the evaluation of the radiation flux components based on the detailed flowfield given by the three-dimensional code and the proper estimate of a view factor. The flame emissivity used in the calculations is dependent on the hydrogen content of the fuel. In addition to the data evaluation effort, the combustor model was used to define the changes needed in the system to alleviate the unfavorable characteristics brought by the high-density fuels. An improved fuel injection concept and primary zone mixing are the main modifications suggested to achieve acceptable performance.

Nomenclature

F = fraction of combustor air to primary zone
F_v = view factor in radiation
L_u = luminosity factor in gas emissivity equation
m_B = fuel fraction burned in subvolume
LHV = lower heating value of fuel, kJ/kg
P_3 = liner inlet air pressure, kPa
T_u = turbulence characteristics term
V = volume, m^3
$W_{a3.1}$ = liner airflow rate, kg/s
ϵg = gas emissivity
σ_f = surface tension of fuel, N/m
η_c = combustion efficiency

Introduction

EXTENSIVE application of analytical models has been used as a design aid in the development phases of gas turbine combustors. These models account for the various physical and chemical processes occurring within the flowfield, including turbulence and scalar transport, spray dynamics, evaporation and mixing, and hydrocarbon combustion chemistry.[1] An essential requirement of the combustor modeling activity is to predict the performance of the combustor with reasonable accuracy. Significant advances are needed, however, in physical submodels, numerics, and in the mathematical simulation of practical gas turbine hardware. This is necessary to enhance the model capability to accurately evaluate the complex reacting flow encountered in the combustors. Consequently, it is difficult at this stage to analytically predict important design parameters, such as exit pattern factor, flame stability, and ignition, with relatively limited computational domain.

On the other hand, adopting a typical empirical approach to the design of a gas turbine combustor and the prediction of its performance relies on the efficient use of the available experience and wide data base. Empirical correlations have been applied to a large number of combustor configurations operating on typical and alternate fuels.[2,3] In order to successfully employ these correlations to predict various combustor parameters of a certain design, an engineering estimation is required of a number of combustor features. This step is greatly facilitated if sufficient data are available for this particular application. The obvious advantages offered by the empirical approach are the simplicity and the capability to predict the performance of a combustor at any required power mode. The applicability of the approach could be easily extended to other types of fuel provided that their relevant physical and chemical properties are known.

The empirical methods, however, exhibit limitations in a number of critical areas, in particular in guiding the development effort to enhance the performance of an existing combustor and in achieving significant advances in technology. Also, the applicability of an empirical method developed for certain conventional design may not always be suitable to novel or revolutionary combustor concepts.

To use the detailed representation of the flow and combustion processes made available through the analytical codes, and the predictive tool of the proven empirical correlations, a combustor model was formulated.[4] By this means, sophisticated combustion and flow models are brought closer in representing practical combustor components. Their great capabilities to reflect the effect of the modification to combustor design on performance are fully utilized.

The developed performance model was verified by applying the method to a number of production combustors that varied significantly in design and concept. They represented various classes of can-annular and through and reverse flow annular combustors. Satisfactory agreement between the model predictions and the experimental data was obtained under various operating conditions and for typical aviation fuels.[5]

In recent years, the trend to use heavier fuels in gas turbines due to the decreased availability of lighter feedstocks and the strategic benefit of increasing aircraft range has brought interest in high-density fuels. In order to determine the effects of property variations of the high-density fuels on the performance and durability of gas turbine combustion systems, an extensive testing on a single-can combustor rig was performed for JP-4 type fuel and four high-density fuels.[6] Some of the important physical and chemical properties of these fuels are presented in Table 1, and the design features of the combustor are shown in Fig. 1.

The fuel injector used is an air-assist, dual orifice pressure type with fuel-flow rates for the pilot and main circuits of

Presented as Paper 89-0219 at the AIAA 27th Aerospace Sciences Meeting, Reno, NV, Jan. 9–12, 1989; received Jan. 23, 1989; revision received April 30, 1989.

*Staff Research Scientist, Allison Gas Turbine Division. Member AIAA.

†Chief, Combustors Research and Development, Allison Gas Turbine Division. Member AIAA.

Table 1 Test fuel properties

Property	JP-4 POSF-2415	HDF-1 POSF-2383	HDF-2 POSF-2893	HDF-3 POSF-2414	HDF-4 POSF-2429
Lower heating value					
kJ/m^3	3.287×10^7	3.626×10^7	3.645×10^7	3.669×10^7	3.653×10^7
kJ/kg	43,687	42,661	42,526	42,305	42,240
Density, kg/m^3 at 313 K	733	838	845	855	875
Kinematic viscosity, m^2/s at 313 K	0.73×10^{-6}	1.76×10^{-6}	1.77×10^{-6}	1.75×10^{-6}	2.01×10^{-6}
Surface tension, N/m at 313 K	0.0181	0.024	0.0242	0.0244	0.0251
Distillation, K					
Initial boiling point	296	355	361	383	373
10% recovery	343	433	438	441	456
20% recovery	366	455	457	460	465
50% recovery	410	487	489	493	489
90% recovery	505	554	555	560	534
End point	577	682	666	684	683
Hydrocarbon type, vol%					
Paraffins	64.0	14.5	14.2	14.2	1.3
Monocycloparaffins	23.6	35.9	30.6	26.3	20.8
Dicycloparaffins	2.7	35.6	34.3	26.6	56.0
Alkylbenzenes	7.3	8.2	10.8	15.3	7.2
Indans and tetralins	1.0	4.7	8.4	14.5	13.1
Naphthalenes	0.8	0.6	0.9	2.3	0.9
Olefins	0.7	0.4	0.8	0.7	0.7
Hydrogen content, wt%	14.47	13.31	12.93	12.38	12.47
Smoke point, mm	28.0	15.0	13.0	10.0	12.0

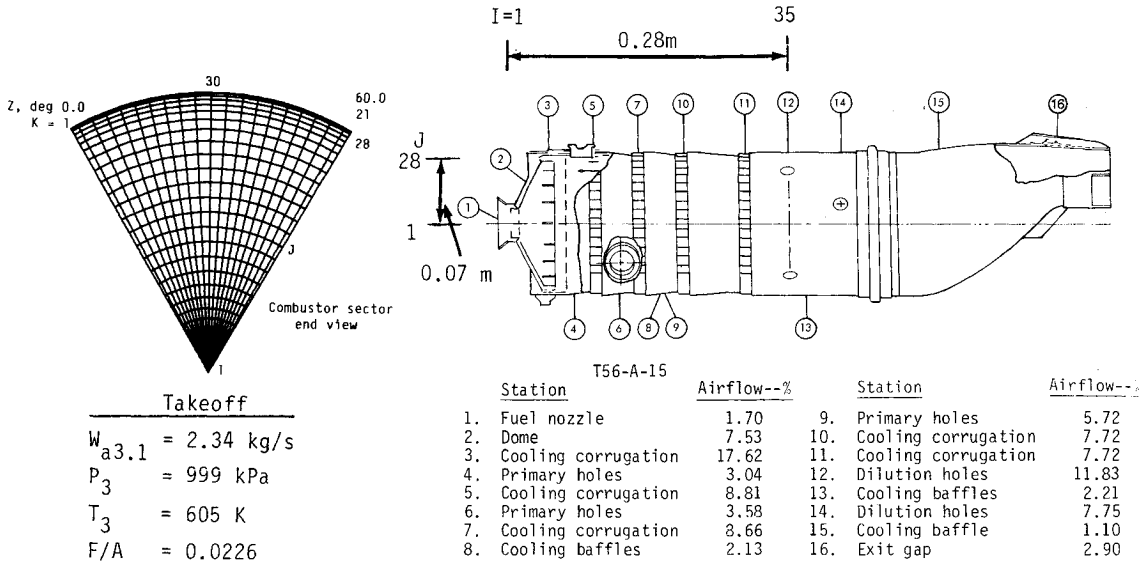

Station		Airflow--%	Station		Airflow--%
1.	Fuel nozzle	1.70	9.	Primary holes	5.72
2.	Dome	7.53	10.	Cooling corrugation	7.72
3.	Cooling corrugation	17.62	11.	Cooling corrugation	7.72
4.	Primary holes	3.04	12.	Dilution holes	11.83
5.	Cooling corrugation	8.81	13.	Cooling baffles	2.21
6.	Primary holes	3.58	14.	Dilution holes	7.75
7.	Cooling corrugation	8.66	15.	Cooling baffle	1.10
8.	Cooling baffles	2.13	16.	Exit gap	2.90

Fig. 1 T56-A-15 combustor flow pattern and node configuration.

0.006 kg/s and 0.027 kg/s, respectively, at a fuel pressure of 0.69 MPa. The injector was tested separately to determine its spray characteristics. At simulated takeoff power mode, the spray angle varied between 70 and 90 deg, and the spray Sauter mean diameter (SMD) was in the range of 35–60 μ, depending on fuel type.[6]

In this program, the developed combustor performance model was utilized to provide insight into the T56-A-15 combustor flowfield and to verify its capability to handle the high-density fuel effects. The model was also used to aid in defining the changes needed in the combustion system to eliminate unfavorable characteristics attributed to the high-density fuels.

Three-Dimensional Combustor Performance Model

A three-dimensional finite-difference code that solves the Navier-Stokes equation for a reacting flowfield is adopted in the combustor performance model. The program simulates turbulence by a two-equation k-ϵ model, and combustion following vaporization is determined by a two-step chemical reaction model based on Arrhenius and Eddy breakup concepts.[7] Extensive improvements in the code included the development of a more flexible grid system and the incorporation of an evaporation model[8] extended to address the relevant properties of the high-density fuels.

To use the output data of the three-dimensional code fully, a feature is introduced into the code that allows the modeled combustor sector to be divided into a large number of subvolumes. The relevant combustion and flow characteristics within each subvolume are evaluated and prepared for use as an input to the performance correlations. The contribution of each subvolume to the overall combustor performance is evaluated using the combustion and flow characteristics within this subvolume as an input to the empirical correlations.

A 60-deg sector of the can combustor was selected for modeling and was divided into $40 \times 28 \times 21$ finite-difference nodes along axial, radial, and circumferential directions, respectively, as shown in Fig. 1. The various parameters calculated in the subvolumes, such as fuel/air ratio (F/A), gas temperature, and fraction of fuel burned, are plotted in Fig. 2 for the HDF-3 fuel along a longitudinal slice through the combustor sector. Figure 3 shows the contours of fuel burned in the sector slice for JP-4.

Comparing these figures indicates that the fuel properties relevant to the atomization and evaporation significantly impact the resulting flowfield. For example, an appreciable amount of fuel is burned near the wall of the primary zone with the HDF-3. This implies that the high-density spray of larger SMD and lower evaporation rate had a better chance to penetrate the recirculation zone and reach these regions than that of JP-4. These differences in flowfield will certainly influence the overall performance of the combustor.

Emissions Predictions

The performance model was applied to the T56-A-15 engine combustor to predict CO, unburned hydrocarbons (UHC), NO_X, and smoke emissions for the high-density fuels. The exhaust concentration of these pollutants was assumed in Ref. 3 to be governed by the mean residence time in the combustion zone, the chemical reaction rates, and the mixing rates. The calculation required estimating a combustion volume and a fraction of air to the primary zone that gave best correlation with the data. Since detailed information on the combustor flowfield is provided by analytical codes, the integration of proven correlations with the codes eliminates the need to estimate these parameters. Thus, the present approach could be applied to predict the performance of current as well as new combustors. The correlations developed in the present effort, based on those reported in Ref. 3 and modified to utilize the three-dimensional code parameters, are given by the following:

$$\mathrm{CO(g/kg)} = \frac{0.0093}{P_3^{1.5}} \left[\frac{m_A m_B T e^{-0.0023T}}{V(1 - m_{ev}/m_F) T_u^{0.5}} \right]_{ijk} \tag{1}$$

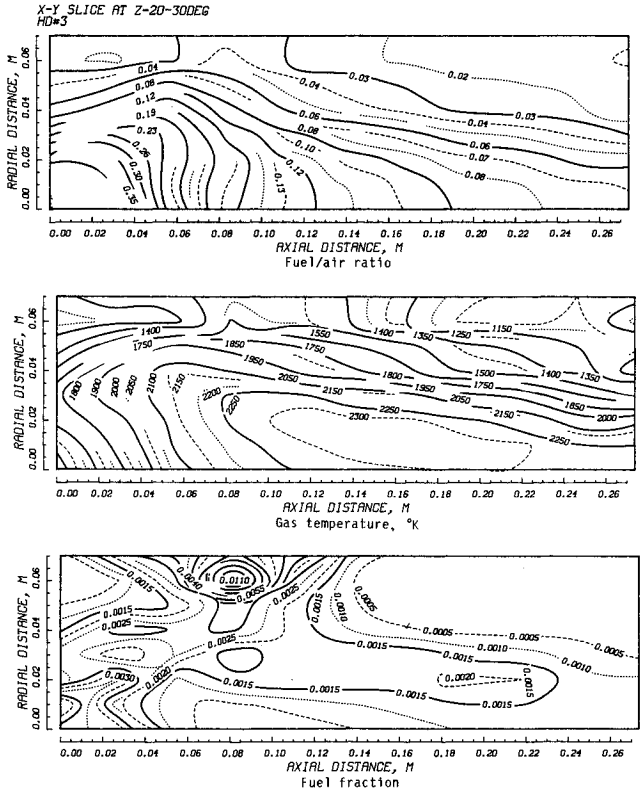

Fig. 2 Combustor flowfield parameters for HDF-3.

and

$$\mathrm{NO_x(g/kg)} = 15.0 P_3^{1.25} \left[\frac{V m_B e^{0.003T}}{T m_A} \right]_{ijk} \tag{2}$$

The expressions within the brackets, as provided by the three-dimensional code, are summed over each of the control volume units. The T is gas temperature, m_A is air-flow rate, and m_F is fuel-flow rate. Fuel-mass fractions evaporated and burned within each subvolume are represented by m_{ev} and m_B, respectively. The mass fraction m_B provides a means to govern the contribution from each unit to the overall combustor performance. The T_u is a parameter to describe mixing rate and is proportional to the eddy diffusivity, mixing area, and density gradient. Thus, it is based on the kinetic energy of turbulence and its rate of dissipation and airflow within each subvolume. A similar expression for UHC is given in Ref. 6.

The exhaust smoke produced by the combustion system represents the balance between the formation process in fuel-

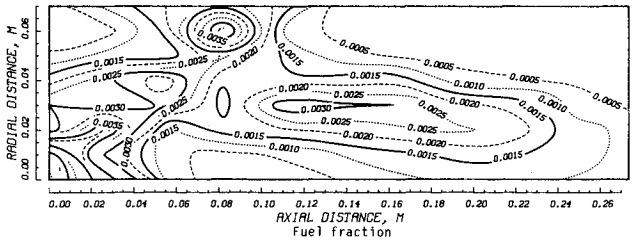

Fig. 3 Combustor flowfield parameters for JP-4.

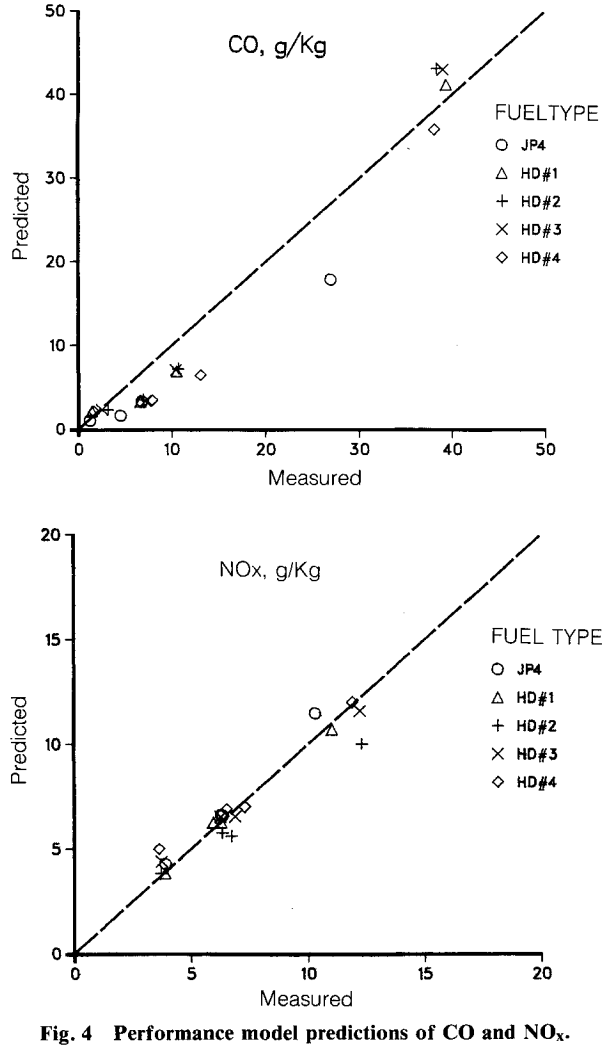

Fig. 4 Performance model predictions of CO and NO_x.

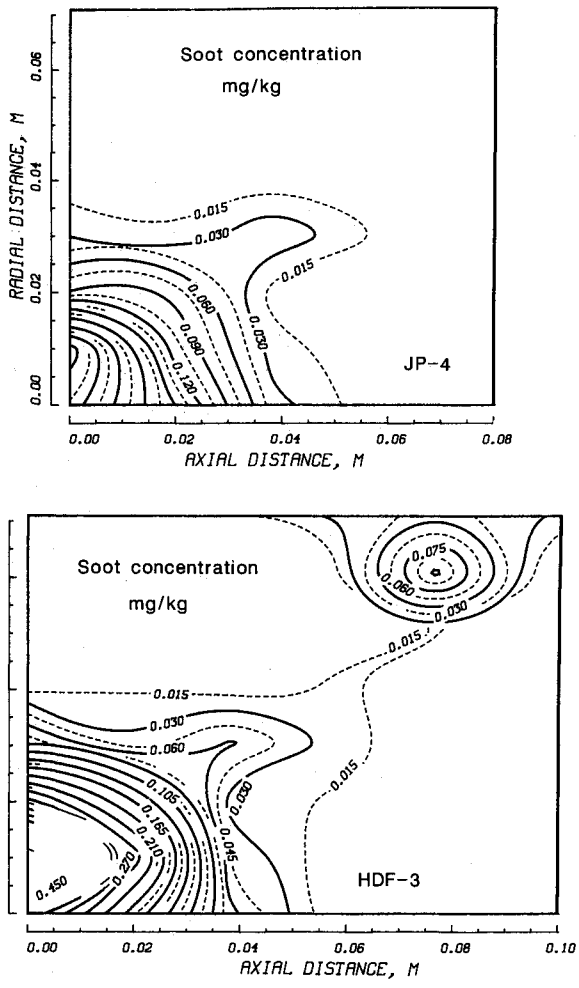

Fig. 5 Contours of soot formation for JP-4 and HDF-3.

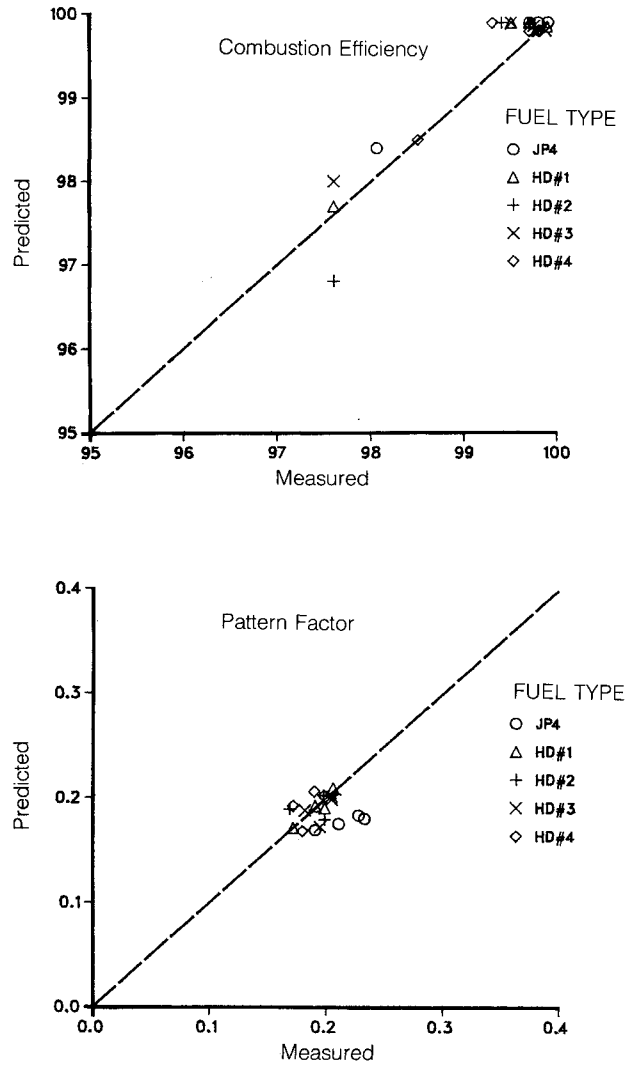

Fig. 6 Model predictions of efficiency and pattern factor.

rich zones that typically exist in the primary zone and soot oxidation in the intermediate zone and possibly the dilution zone. The expressions used to predict the soot formation and oxidation are given by

$$S_F = 0.1773\, P_3^2(18\text{-H})^{1.5} \left[\frac{(F/A)m_B}{Tm_A T_u^{0.25}}\right]_{ijk} \tag{3}$$

$$S_O = 0.042(18\text{-H})^{1.5} \frac{P_3^2}{V}\left(\frac{F/A}{T}\right)_{pz} \left[\frac{Ve^{0.0011T}}{m_A(F/A)}\right]_{ijk} \tag{4}$$

The subscript *pz* indicates average values in the primary zone and H is the hydrogen content in fuel.

The combustor performance model predictions of CO and NO_x are plotted against the measured data in Fig. 4. Good agreement is shown in this figure. In order to define the regions that are responsible for the soot formation in the combustor, contours of soot concentration formed in various zones are plotted in Fig. 5 for JP-4 and HDF-3. This high-density fuel possesses the highest aromatic content and lowest hydrogen content and smoke point among the fuels tested in the program.

It is seen that soot is formed in the very rich zone near the fuel injector for both fuels, and the formation regions extend for the HDF-3 to reach the liner wall. Inadequate mixing in the primary zone, coupled with low quality atomization, are contributing to the high-soot concentration observed in Fig. 5.

Performance Predictions

The three-dimensional code was also combined with the performance correlations to predict parameters such as combustion efficiency, pattern factor, lean blowout (LBO) and ignition characteristics. The main factors affecting the combustion efficiency, as described in Ref. 2, are evaporation, mixing, and reaction rates. The following expression was used to predict the efficiency:

$$\eta_c = \eta_r \eta_{ev} \eta_{mix} \tag{5}$$

where the reaction term is given by

$$\eta_r = 1 - \exp\left(-0.07\, P_3^{1.3}\left[\frac{Vm_B e^{T/400}}{m_A}\right]_{ijk}\right) \tag{6}$$

the evaporation term is

$$\eta_{ev} = 1 - \exp\left(-1.71\left[\frac{m_F m_B}{m_A}\right]_{ijk}\right) \tag{7}$$

and the mixing rate contribution to combustion efficiency is

$$\eta_{mix} = 1 - \exp\left(-\frac{1500}{V}\,[T_u^{0.5}V]_{ijk}\right) \tag{8}$$

The predictions of the combustion efficiency are plotted against the measurements in Fig. 6. The combustor exhaust gases pattern factor was also calculated and compared with the data in the same figure. The correlation developed is based on the evaluation of turbulence characteristics of flow that govern the mixing rate in various zones of the combustor, the length occupied in fuel evaporation L_{ev}, and an equivalent

length of combustor that accounts for the transition section of the liner L_L. The pattern factor (PF) is given by

$$\text{PF} = 1 - \exp - 0.0095\left/\left(\frac{L_L - L_{ev}}{D_L V F_D} \cdot [T_u^{0.5} V]_{ijk}\right)\right. \quad (9)$$

where D_L is the combustor diameter and F_D is a factor defining the temperature profile in the dilution zone. This approach indicates that achieving low PF requires improved mixing in the combustion zone as well as in the dilution zone. The correlation also enhances the pattern factor prediction since the analytical treatment of a single combustor sector cannot accurately represent the overall exit gas temperature pattern of the combustor.

In order to utilize the multidimensional calculations in predicting fuel/air ratio at LBO, the evaporation characteristics at the conditions employed in the three-dimensional analysis are converted into the corresponding characteristics at LBO conditions through a parameter t_r. This parameter is based on the ratio of the evaporation times at the two operating conditions as determined from the evaluation of the values of the SMD and evaporation constant. An iterative procedure is adopted in the calculation to estimate the values of these parameters at an assumed value of LBO fuel/air ratio and to verify the assumption using the following expression:

$$\text{LBO } F/A = \frac{98{,}000}{\text{LHV}} P_{3\text{des}} \left(\frac{FW_{a3} t_r}{P_3^{1.3} e^{T/300}}\right) \cdot \left[\frac{m_{ev} m_B}{T m_A m_F}\right]_{ijk} \quad (10)$$

The F is the fraction of air based on average fuel/air ratio in the primary zone, and $P_{3\text{des}}$ is the pressure used in the three-dimensional analysis. Lean flame extinction tests were performed at subidle conditions, and a number of data points were recorded for each fuel to ensure repeatability of data. Figure 7 shows the LBO characteristics of the JP-4 and the four high-density fuels as given by the model plotted against the data.

Similar procedure was followed to evaluate the ground ignition and altitude relight fuel/air ratio.[6] The results of the calculations of the JP-4, together with those of the HDF-4, which possessed the highest viscosity and surface tension among the fuel tested, are plotted also in Fig. 7.

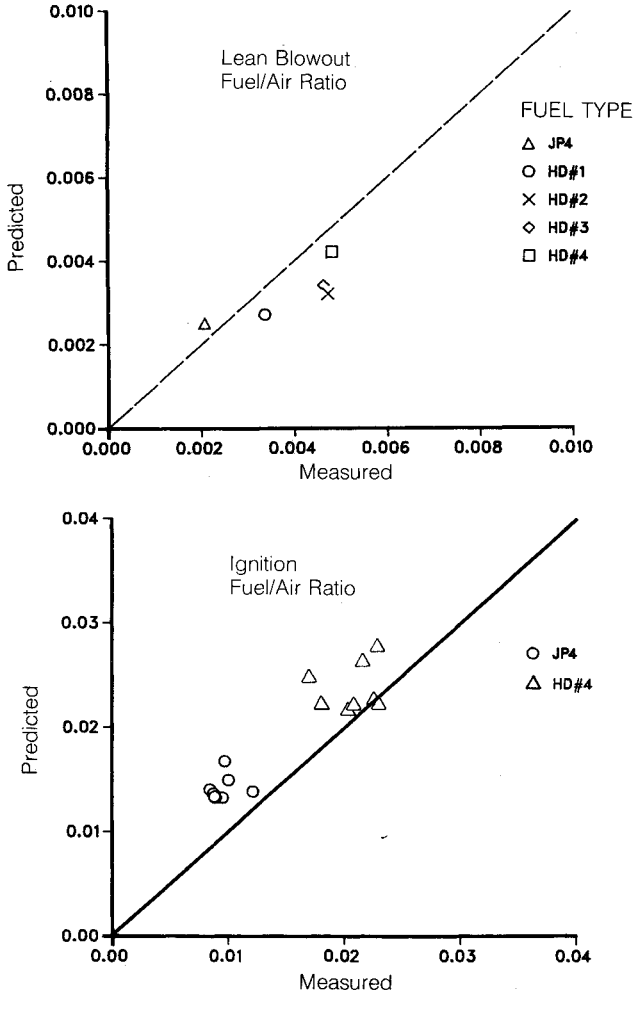

Fig. 7 Model predictions of lean blowout and ignition.

Combustor Dome and Liner Temperatures

The effects of burning the high-density fuels on the T56-A-15 liner wall temperature were determined by combustor rig testing and heat transfer analysis. Thermal paint testing, followed by temperature measurement with 30 thermocouples distributed on dome, liner, and transition sections were carried out for all the fuels.

In the heat transfer analysis, the liner is heated by the radiation from the flame and hot gases and convection from the gas flow within the chamber. The removal of heat from the burner walls occurs through radiation to the outer casing and convection to the annulus air and is supplemented by the film cooling concept adopted in the combustor design.

The gas emissivity in the analysis is calculated from the knowledge of the beam length that is determined by the size and shape of the gas volume, gas properties, and a luminosity factor L_u given by

$$L_u = 5.964 \times 10^8 / \text{H}^{7.365} \quad (11)$$

where H is the hydrogen content of the fuel. This factor, which gave better fit to a wide data base, was used in the calculation of nonluminous flame gas emissivity to account for the presence of soot particles in the flame.

In order to accurately predict liner hot streaks, the radiation flux contribution from various combustor zones onto each wall segment was calculated from the detailed three-dimensional flowfield in addition to a means of defining a radiation view factor F_v. Adopting this concept, the radiation flux to a wall segment was calculated using the following equation[3,4]:

$$R = 0.5\sigma(1 + \epsilon_w)\Sigma[F_v \epsilon g T^{1.5}(T^{2.5} - T_w^{2.5})]_{ijk} \quad (12)$$

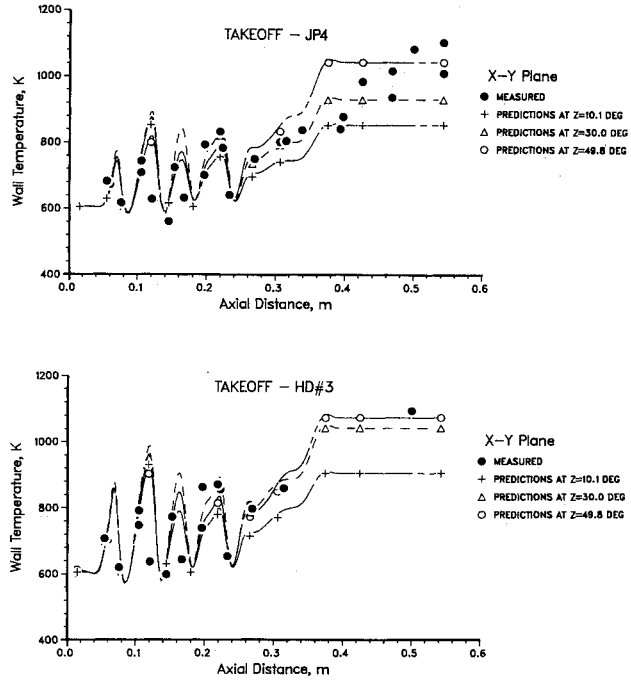

Fig. 8 Heat transfer model predictions for JP-4 and HDF-3.

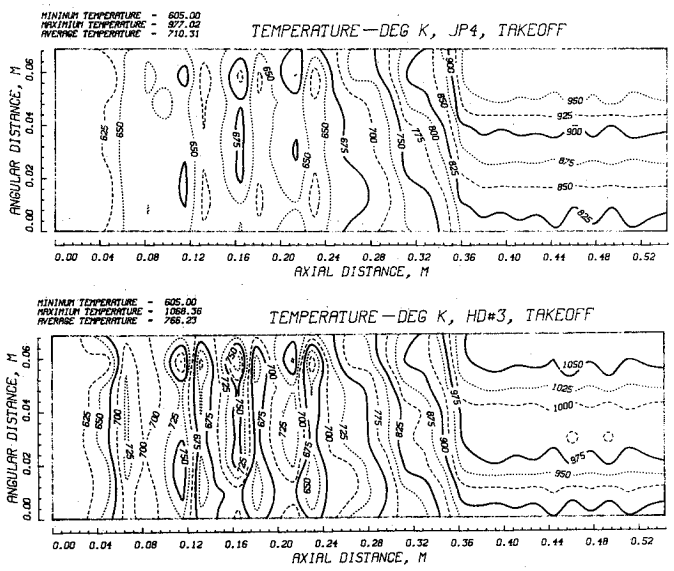

Fig. 9 Contours of wall temperatures for JP-4 and HDF-3.

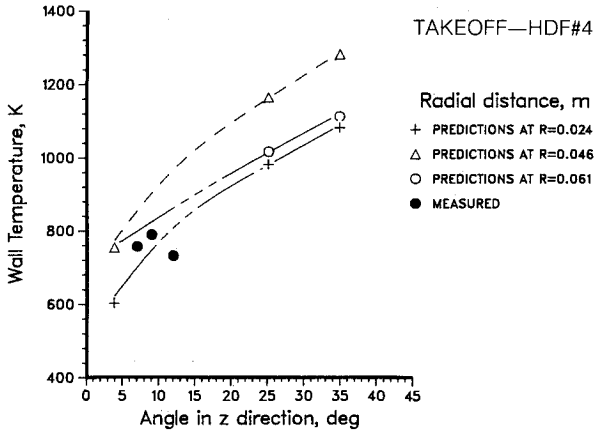

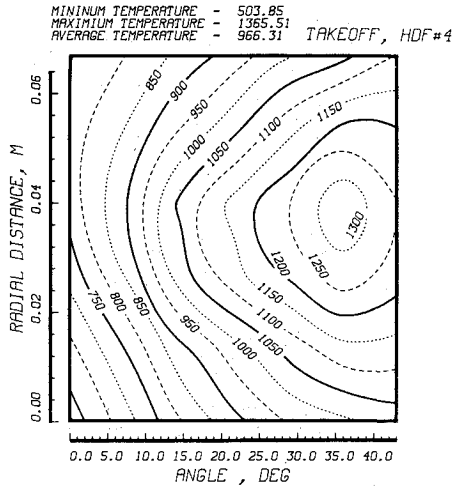

Fig. 10 Contours of dome temperatures.

where the terms within the brackets are based on local properties within each combustor zone, as given by the three-dimensional code. The ϵ_w is wall emissivity that depends on material, temperature, and degree of oxidation of the wall, and σ is the Stefan-Boltzmann constant.

The internal convection component calculation is based on the adiabatic gas temperature that is obtained from the definition of the film cooling effectiveness.[9] The calculation of the

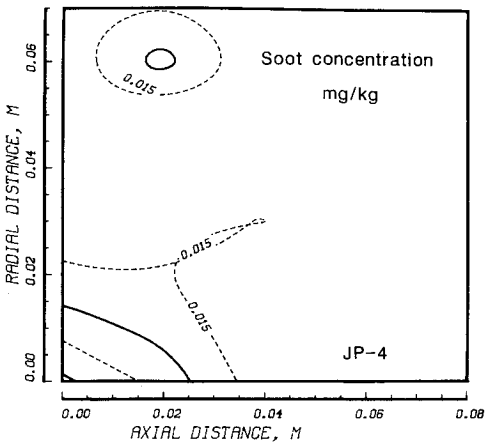

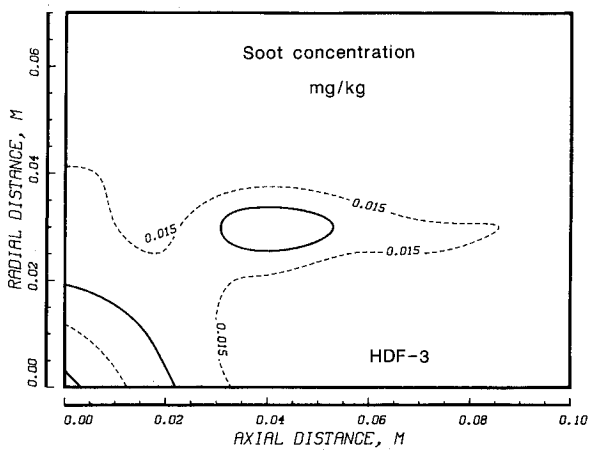

Fig. 11 Contours of soot formation of proposed combustor.

wall temperature is performed by balancing the heat fluxes on a wall segment through an iterative procedure, and a wall conduction component is used to determine the temperature gradient across the segment.

The wall temperature at three axial planes of the combustor sector is given in Fig. 8 for JP-4 and HDF-3 at takeoff conditions. The thermocouple measurements are also plotted in the figure. It is obvious that the utilization of the three-dimensional variation in combustor internal parameters leads to a good correlation with the data.

To obtain a detailed picture of the temperature variation in both the axial and circumferential directions, the temperature contours of the unwrapped sector are plotted in Fig. 9. The vertical axis in this figure indicates the linear distance of the unwrapped wall sector measured from one side of the sector up to the maximum value corresponding to 60 deg. From this figure, one can see the locations of hot and cold regions and the higher temperature levels obtained with the high-density fuel. Gas temperature, air distribution within and around the liner, and the location relative to a cooling slot are the main factors responsible for the wall temperature trends observed in this figure.

The dome temperature distribution plotted against the distance from the exit plane of a dome cooling baffle is shown in Fig. 10 for a number of radii. The measurements are also included in the figure. Contours of dome temperatures on a segment of the dome are included in the figure.

Combustion System Modification

According to the data evaluation phase of the present investigation, the T56-A-15 combustor produced excessively high levels of smoke, demonstrated increased levels of flame stability and altitude relight fuel/air ratios, and experienced hotter

wall temperatures in the primary zone when operating on the high-density fuels.

An effective approach to these performance problems posed by the high-density fuels would aim at improving the atomization quality and the fuel/air mixing in the combustor primary zone. The direct effect would be a significant reduction in soot formation with a simultaneous control of wall temperature problems. The improved primary zone aerodynamics, coupled with a rapid evaporation rate of the finer spray, would result in better flame stability, starting, and altitude relight performance.

Improved cooling techniques with enhanced effectiveness could maintain acceptable wall temperatures over the hydrogen content range of the high-density fuels. This, coupled with appropriate cooling air distribution to various combustor zones would certainly achieve the liner-life goal when utilizing these alternate fuels.

Based on the above consideration, several modifications to the combustor were recommended. A piloted airblast atomizer should replace the existing dual-orifice type to improve quality of atomization. A dome swirler that encloses the atomizer, in addition to an air shroud, is suggested in the modified design to enhance overall fuel/air mixing in the primary zone.

In order to maintain a proper stoichiometry in the primary zone, enlarged holes of the first row are proposed in the design. A convection/film cooling concept with redistributed cooling air to different combustor zones is adopted in the new design. The new configuration was used in the three-dimensional performance model to demonstrate the extent of improvement over the current design.

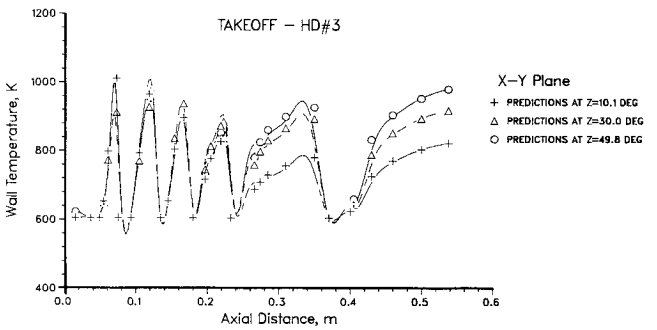

Fig. 12 Wall temperature predictions of proposed combustor.

Examining the three-dimensional flowfield results revealed a reduction in the levels of fuel/air ratio downstream of the atomizer compared to the corresponding results of the original design. Higher gas temperatures in this region and considerable reduction in the fraction of fuel burned near the liner walls are also observed with the modified design. The direct results of all of these factors are a significant reduction in soot formation. This is obvious in Fig. 11, which depicts the soot-formation contours for JP-4 and HDF-3.

The improved atomization and evaporation characteristics are reflected in the enhanced combustor performance predictions as given by the model and included in Table 2. In this table, the overall performance of the combustor, as measured on the test rig, is compared with the model predictions. Ignition and relight tests were performed at a number of different flow conditions. The anticipated performance of the proposed liner, as given by the model at the same test conditions, is also included in the table. The wall temperature predictions are given in Fig. 12 for the HDF-3 which has the lowest hydrogen content in the fuel tested. Reduction in the peak temperatures is predicted for the modified cooling configuration.

Conclusions

The application of the combustor performance model to predict the performance of the T56-A-15 combustor when operating on the high-density fuels proved to be very encouraging. This model combines the analytical capabilities of the three-dimensional combustor codes to define the flowfield with the proven empirical correlations. The model validation effort, therefore, was taken a step further ahead to include the effects of alternate fuels, in addition to the extensive application to various combustor designs.

The advantage offered by the performance model is the capability to sense the impact of a systematic modification to the details of the combustor on its performance. Moreover, the model can be easily employed to detect the regions in the combustor responsible for any observed trends in performance. It also eliminates the need for engineering estimates of certain combustor parameters.

A demonstration run using the combustor performance model was performed for a proposed combustor configuration that alleviates the problems associated with burning the high-density fuels. The predictions showed that satisfactory levels of performance and liner wall temperature could be achieved for the modified liner.

Table 2 Predictions of performance of modified combustor

	JP-4			HDF-3		
	T56-A-15		Proposed liner	T56-A-15		Proposed liner
	Measured	Predicted	Predicted	Measured	Predicted	Predicted
Sea-level takeoff						
CO, g/kg	1.16	0.97	1.15	2.46	2.25	1.9
UHC, g/kg	0.09	0.33	0.36	0.12	0.74	0.62
NO_x, g/kg	10.28	11.45	15.9	12.19	11.57	15.6
Smoke SAE no.	37.0	32.6	<5.0	53.3	51.4	<5.0
Combustion efficiency	0.999	0.999	0.999	0.999	0.999	0.997
Pattern factor	0.23	0.18	0.13	0.204	0.20	0.14
Lean blowout F/A[a]	0.0021	0.0025	0.0012	0.0047	0.0034	0.0015
Altitude relight F/A[a]	0.0097	0.0167	0.0061	0.025	0.0227	0.0102
	0.0088	0.0133	0.0034	0.0156	0.0174	0.0057
	0.0121	0.0138	0.0045	0.021	0.0191	0.0048
Sea-level ignition F/A[a]	0.010	0.0149	0.006	0.0176	0.0184	0.0102
	0.0089	0.0132	0.0042	0.0143	0.0164	0.0074
	0.0095	0.0132	0.0033	0.0151	0.0174	0.0056
	0.0087	0.0136	0.0025	0.0166	0.0165	0.0047
	0.014	0.0084	0.0022	0.0191	0.0174	0.0040

[a]Fuel/air.

Acknowledgments

This work was conducted under U.S. Air Force Contract F33615-86-C-2604. The Air Force Technical Monitor on this program was Curtis Reeves.

References

[1]Mongia, H. C., Reynolds, R. S., and Srinivasan, R., "Multidimensional Gas Turbine Combustion Modeling: Applications and Limitations," *AIAA Journal,* Vol. 24, No. 6, June 1986, pp. 890–904.

[2]Lefebvre, A. H., "Fuel Effects on Gas Turbine Combustion-Ignition, Stability, and Combustion Efficiency," *ASME Journal of Engineering for Gas Turbine and Power,* Vol. 107, Jan. 1985, pp. 24–37.

[3]Lefebvre, A. H., "Fuel Effects on Gas Turbine Combustion-Liner Temperature, Pattern Factor, and Pollutant Emissions," *Journal of Aircraft,* Vol. 21, No. 11, Nov. 1984, pp. 887–898.

[4]Rizk, N. K., and Mongia, H. C., "Gas Turbine Combustion Design Methodology," AIAA Paper 86-1531, 1986.

[5]Mongia, H. C., "A Status Report on Gas Turbine Combustion Modeling," *AGARD Conference Proceedings,* No. 422, Oct. 1987.

[6]Rizk, N. K., Oechsle, V. L., Ross, P. T., and Mongia, H. C., "High Density Fuel Effects," Air Force Wright Aeronautical Lab., Wright-Patterson AFB, OH, AFWAL-TR-88-2046, Aug. 1988.

[7]Mongia, H. C., and Reynolds, R. S., "Combustor Design Criteria Validation," Vol. III, U.S. Army Research and Technology Lab., USARTL-TR-78-SSC, Feb. 1979.

[8]Faeth, G. M., "Current Status of Droplet and Liquid Combustion," *Progress in Energy and Combustion Science,* Vol. 3, Pergamon, London, 1977, pp. 191–224.

[9]Lefebvre, A. H., *Gas Turbine Combustion*, McGraw-Hill, New York, 1983, pp. 257–320.